JOURNAL OF
CUTANEOUS IMMUNOLOGY
AND ALLERGY

TYPE Original Research
PUBLISHED 18 September 2026
DOI 10.3389/jcia.2026.17310

OPEN ACCESS

*CORRESPONDENCE
Naoya Kase,
naoya.kase@rs.tus.ac.jp
Yohsuke Harada,
yohsuke@rs.tus.ac.jp

RECEIVED 06 July 2026
REVISED 13 August 2026
ACCEPTED 31 August 2026
PUBLISHED 18 September 2026

CITATION
Kase N, Nakamura H, Nakakomi C, Shimakata M, Banno M, Kanari R and Harada Y (2026) Cross-species gene expression analysis identifies a type I interferon-associated transcriptional signature in Tregs from atopic dermatitis. *J. Cutan. Immunol. Allergy* 9:17310. doi: 10.3389/jcia.2026.17310

Cross-species gene expression analysis identifies a type I interferon-associated transcriptional signature in Tregs from atopic dermatitis

Naoya Kase*, Hina Nakamura, Chizuru Nakakomi, Manami Shimakata, Mai Banno, Ryotaro Kanari and Yohsuke Harada*

Department of Medicinal and Life Sciences, Faculty of Pharmaceutical Sciences, Tokyo University of Science, Tokyo, Japan

Although regulatory T cells (Tregs) maintain immune tolerance, disease-relevant Treg molecular states in atopic dermatitis (AD) remain unclear. This study used an inducible mouse model of spontaneous AD-like dermatitis caused by combined *Foxp3* and *Bcl6* gene deletion and established a bacterial artificial chromosome reporter system to track Tregs after *Foxp3* loss. Bulk RNA sequencing (RNA-seq) of splenic Tregs revealed robust induction of antiviral and type I interferon (IFN)-responsive gene programs in *Foxp3*/*Bcl6*-deficient Tregs. To assess its clinical relevance, single-cell RNA-seq data from patients with AD were reanalyzed. The analysis revealed that the ortholog-mapped mouse signature was selectively enriched in human Tregs, and type I IFN response signatures were elevated. Regulon analysis further implicated IFN-associated transcription factors, including IFN regulatory factor and signal transducer and activator of transcription family members, as candidate regulators of this program. These cross-species results highlight a type I IFN-associated Treg transcriptional state in AD and support the utility of this model for mechanistic studies of Treg-dependent disease processes.

KEYWORDS
atopic dermatitis, gene regulatory networks, interferon, regulatory T cells, RNA sequencing

Introduction

Atopic dermatitis (AD) is a chronic inflammatory skin disorder caused by complex interplay between skin barrier disruption and immune dysregulation [1]. Among the immunological abnormalities implicated in its pathogenesis, type 2 immune responses play a central role [2]. In particular, the monoclonal antibody dupilumab, which targets interleukin four receptor, has shown substantial clinical efficacy, thereby emphasizing the importance of type 2 cytokine signaling in this disease [3, 4]. However, the use of dupilumab is limited by the side effects of ocular complications [5] and the economic burden inherent to antibody-based therapies [6]. Therefore, safe and affordable therapeutic strategies that target the pathogenic mechanisms underlying AD are urgently needed.

Regulatory T cells (Tregs) are essential for maintaining immune tolerance [7] and contribute to disease progression. Hence, Tregs may represent therapeutic targets in AD [8].

Notably, Treg numbers increase in proportion to disease severity [9, 10]. This suggests that Tregs may be functionally altered rather than simply expanded. Such abnormalities are associated with changes in Treg gene expression, which potentially reflects the dysregulation of forkhead box P3 (FOXP3) [11]. This master transcription factor governs Treg identity and function [7]. However, determining the causal relationship between transcriptional abnormalities and disease pathogenesis in patients exposed to chronic inflammatory conditions and diverse therapeutic interventions remains difficult. Thus, analyses based solely on patient-derived data have inherent limitations. This highlights the importance of animal models in mechanistic investigations.

The MC903-induced mouse model is currently the most widely used AD mouse model [12]. Although topical application of MC903 rapidly induces dermatitis and type 2 immune responses characteristic of AD, this model is driven by an exogenous pharmacological stimulus [13]. Therefore, the model may not be suitable for investigating disease processes associated with abnormalities in immune cells [14]. Moreover, considering that topical application of MC903 does not induce dermatitis in humans [15], this model is not completely applicable to human disease conditions. Simultaneous loss of *Foxp3* and *Bcl6* induces a spontaneous AD-like phenotype [16, 17]. Given that *Bcl6* and *Foxp3* play an important role in maintaining Treg function [18], this finding strongly suggests that Tregs lacking both genes contribute to the pathogenesis of AD. Unlike disease progression in the MC903 model, the disease in this gene deletion model emerges spontaneously several weeks after gene deletion [16]. This provides an opportunity to track dynamic changes in immune cell states before the onset of overt dermatitis. Thus, this model may be useful for investigating the immune cell-associated mechanisms of AD. However, a direct comparison between this model and human AD, particularly at the level of Treg gene expression, has not yet been performed.

Accordingly, this study shows that changes in Treg gene expression induced by the systemic deficiency of *Foxp3* and *Bcl6* are accompanied by a transcriptional program closely associated with Tregs in patients with AD. The study first developed a mouse model that enabled the tracking of Tregs with the potential to express *Foxp3* even after *Foxp3* deletion. Subsequently, transcriptomic analysis of Tregs isolated using this system revealed that the combined loss of these two genes unexpectedly elevated the type I interferon (IFN)-associated gene signature. Furthermore, analysis of patient-derived single-cell transcriptomic data also elevated of the type I IFN-associated gene signature in patient Tregs. The analysis also suggested the involvement of IFN regulatory factor (IRF) 7 as a candidate upstream transcriptional regulator. Collectively, these findings indicate that the Treg gene expression program induced by systemic *Foxp3* and *Bcl6* deficiency recapitulates the key features of patient Tregs and supports the utility of this model for dissecting Treg-dependent mechanisms underlying AD.

Materials and methods

Mice

To generate F-KO-BAC and F-B-KO-BAC mice, F-KO and FB-KO C57BL/6 mice [16] were crossed with BAC C57BL/6 mice provided by Dr. Günter J. Hämmerling [19]. The mice were maintained under specific pathogen-free conditions at the animal facilities of the Tokyo University of Science. For gene knockout, approximately 2 mg of tamoxifen (19885-34, Nacalai Tesque, Kyoto, Japan) solubilized in corn oil (032-17016, FUJIFILM Wako Pure Chemical, Osaka, Japan) was orally administered to mice once every 2 days for a total of six administrations.

Flow cytometry and cell sorting

Collected spleens were mechanically dissociated using frosted microscope slides (S2226, Matsunami Glass Industry, Osaka, Japan) and suspended in FACS buffer containing 1% fetal bovine serum, 0.05% sodium azide (197-11091, FUJIFILM Wako Pure Chemical), and 2 mM EDTA (311-90075, Nippon Gene, Tokyo, Japan). The cell suspensions were passed through a 40-μm cell strainer to obtain single-cell suspensions. This was followed by red blood cell lysis using buffer containing 0.15 M ammonium chloride (017-02995, FUJIFILM Wako Pure Chemical), 10 mM potassium hydrogen carbonate (166-03275, FUJIFILM Wako Pure Chemical), and 0.1 mM Na_2EDTA (345-01865, Dojindo, Tokyo, Japan). For skin cells, samples were collected from lesional areas of FB-KO-BAC mice and processed into single-cell suspensions as previously described with minor modifications [20]. Briefly, skin tissues were minced into small pieces and enzymatically digested by RPMI (189-02025. FUJIFILM Wako Pure Chemical) containing 200 μg/mL Liberase TL (05401020001, Merck, Darmstadt, Germany) and 5 μg/mL DNaseI (DM25, Merck). The cell suspensions were passed through a 70-μm cell strainer to obtain single-cell suspensions and resuspended FACS buffer containing 5% fetal bovine serum, 0.05% sodium azide, and 2 mM EDTA. The cells were stained with the antibodies listed below and Fixable Viability Dye eFluor™ 506 (65-0866-14, Thermo Fisher Scientific, Waltham, MA, USA) for 30 min. Cells stained with biotin-conjugated antibodies were subsequently incubated with PE/Cyanine7-conjugated streptavidin (25-4317-82, Thermo Fisher Scientific) for an additional 30 min. For intracellular staining, cells were fixed and permeabilized using a FOXP3/Transcription Factor Staining Buffer Set (00-5523-00; Thermo Fisher Scientific) before intracellular antibody staining: PE/Cyanine7 anti-CD4 Antibody (100528, BioLegend, San Diego, CA, USA); Alexa Flour™ 488 anti-FOXP3 Antibody (53-5773-80, Thermo Fisher Scientific); APC/Cyanine7 anti-CD3 Antibody (560590, BioLegend); PE anti-γδTCR Antibody (12-9959-41, Thermo Fisher Scientific); BV421 anti-CTLA4 antibody (106312, BioLegend); Biotin anti-CD25 antibody (102003, BioLegend), PerCP-Cy5.5 anti-CD45 Antibody (550994, BioLegend), APC/Cyanine7 anti-CD90.2 Antibody (105327, BioLegend), Alexa Flour™ 700 anti-CD4 Antibody (557956, BioLegend). The cells were analyzed using a FACS Lyric flow cytometer (BD Biosciences, San Jose, CA, USA) and sorted using a FACS Melody cell sorter (BD Biosciences).

Bulk RNA-seq and analysis

RNA was extracted from the sorted cells using an RNeasy Mini Kit (74104; Qiagen, Hilden, Germany) according to the manufacturer's instructions. RNA-Seq library preparation and sequencing were performed by Azenta Life Sciences (South

Plainfield, NJ, USA) using an Illumina platform. Raw reads were converted to FASTQ files using bcl2fastq v2.20.0.422, and sequencing quality was assessed using FastQC v0.10.1. Adapter sequences and low-quality reads were removed using Cutadapt v1.9.1. The clean reads were aligned to the mouse reference genome, *Mus musculus* GRCm38.101, using HISAT2 v2.2.1. The resulting BAM files were used for downstream quantification. Gene-level read counts were generated using feature counts. DEGs were identified based on an adjusted p-value of <0.05 and a fold change of >1.5. The datasets were deposited at the[1] repository (accession number PRJNA1473592).

Analysis of scRNA-seq

Publicly available PBMC scRNA-seq (GSE189188) data from HCs and patients with AD were reanalyzed using Seurat [21, 22]. Raw 10x Genomics HDF5 feature-barcode matrices were loaded for each sample, and Seurat objects were generated using genes detected in at least three cells and cells expressing at least 200 genes. Cells were retained after quality control based on the following criteria: 200–6,000 detected genes, 500–70,000 RNA counts, and mitochondrial gene content ≤15%. After merging all samples, gene expression was log-normalized. Subsequently, highly variable genes were identified, and T-cell receptor/B-cell receptor genes were removed from the variable feature set. The data were scaled using the regression of total RNA counts and mitochondrial gene percentages, followed by PCA. Sample-level batch effects were corrected using Harmony [23], and UMAP visualization and graph-based clustering were performed using harmony-corrected dimensions. Major PBMC populations were annotated based on canonical marker gene expression and cluster-specific marker genes. T-cell clusters were extracted and reanalyzed independently using the same workflow. This included log normalization, variable feature selection, scaling, PCA, Harmony integration, UMAP visualization, and clustering. T-lineage clusters were annotated based on canonical markers for naïve, memory, activated, cytotoxic, cycling, IFN-high, and Tregs. Non-T-lineage contaminating clusters were excluded, and mouse signature genes were converted to human orthologs using GeneToList [24] and intersected with genes detected in the dataset. The signature scores were calculated using Seurat's AddModule Score function. Differential expression analysis between AD and HC cells was performed using FindMarkers within each T-lineage cluster, and genes ranked according to the average log2 fold change were used for GSEA. Enrichment of the FB-KO-UP-derived human signature was assessed using fgsea, and Hallmark pathway enrichment in Tregs was analyzed using MSigDB Hallmark gene sets with fgsea. Tregs were further subjected to SCENIC [25] analysis to infer transcription factor regulons. The RSS [26] was calculated to compare regulon activity between AD and HC Tregs.

1 https://www.ncbi.nlm.nih.gov/

Statistical analysis

Statistical analyses were performed using GraphPad Prism or R/Bioconductor software packages. Statistical significance was set at $p < 0.05$. Statistical tests used for each experiment are described in the corresponding figure legends.

Results

Establishment of a mouse model enabling green fluorescent protein (GFP)–based tracking of *Foxp3*-deficient Tregs

To enable tracking of Tregs after *Foxp3* deletion, this study established a GFP-based reporter mouse system. F-KO mice were generated on the C57BL/6 background by crossing Foxp3^{flox} mice with Rosa26^{CreERT2} mice, whereas FB-KO mice were generated by crossing Foxp3^{flox} Bcl6^{flox} mice with Rosa26^{CreERT2} mice [16, 17, 27]. These mice were further crossed with Foxp3.LuciDTR bacterial artificial chromosome (BAC) transgenic mice (BAC mice), in which green fluorescent protein, luciferase, and the diphtheria toxin receptor are expressed under the control of the Foxp3 promoter [19]. These crosses generated F-KO-BAC and FB-KO-BAC mice, respectively (Figure 1A). This transgene drives the expression of GFP, luciferase, and diphtheria toxin receptor in a *Foxp3* promoter-dependent manner, regardless of the presence or absence of the endogenous *Foxp3* locus. Therefore, Tregs can be tracked by GFP and luciferase signals, even after tamoxifen-induced deletion of *Foxp3* (Figure 1B). To validate this reporter system, Foxp3 and GFP expression were evaluated in F-KO-BAC mice before and 13 days after the start of tamoxifen administration. In addition, the ability of GFP expression to track Tregs after Foxp3 deletion was assessed. As expected, tamoxifen treatment markedly reduced the frequency of Foxp3$^+$ T cells, as determined by intracellular antibody staining (Figures 1C,D), whereas the frequency of GFP$^+$ T cells was increased (Figures 1E,F). Among CD4$^+$ GFP$^+$ cells sorted from untreated FB-KO-BAC mice, the majority were CD3$^+$, Foxp3$^+$, CD25^{high}, and γδTCR$^-$, and CTLA-4 expression was enriched compared with the GFP$^-$ population, although a small fraction of CD4$^+$ Foxp3$^-$ cells with an unexpected phenotype was also detected (Supplementary Figure 1). These findings indicate that GFP expression predominantly identifies cells with a conventional Treg phenotype and supports the use of this mouse model for GFP$^-$ based tracking of Tregs after inducible Foxp3 deletion.

Transcriptome analysis of GFP$^+$ cells in FB-KO-BAC mice

GFP$^+$ cells were detected in the lesional skin of FB-KO-BAC mice, suggesting that Treg$^-$ derived cells accumulated at the site of inflammation (Supplementary Figure 2). To characterize gene expression changes in Tregs from FB-KO-BAC mice, splenic GFP$^+$ cells were sorted 14 days after the start of tamoxifen administration, and RNA sequencing (RNA-seq) analysis was performed. Principal component analysis (PCA) revealed that the GFP$^+$ cells derived from BAC, F-KO-BAC, and FB-KO-BAC mice exhibited distinct gene expression profiles (Figure 2A). Furthermore, differentially expressed genes (DEG) were identified among these groups, and 144 genes that

10.3389/jcia.2026.17310

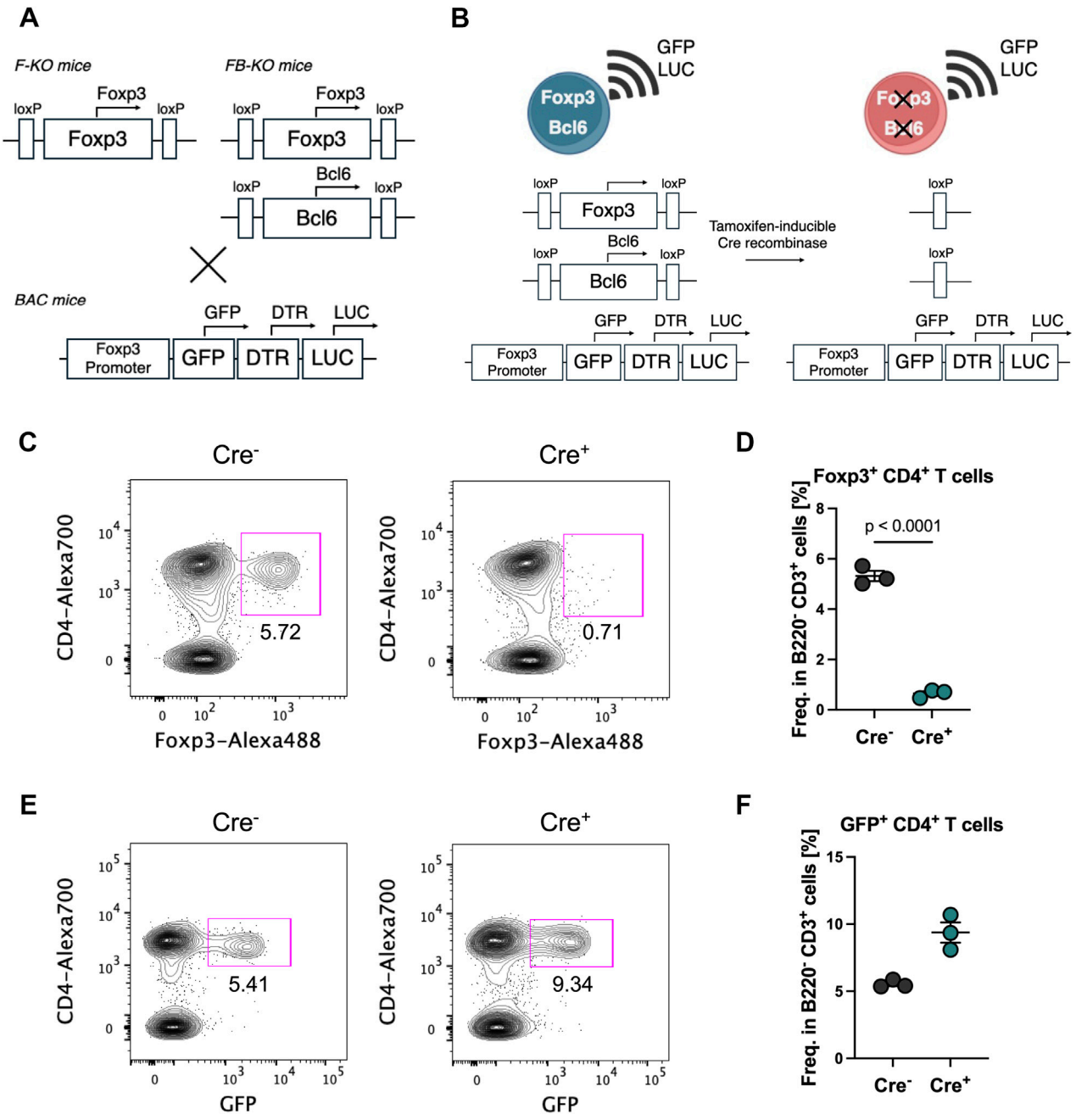

FIGURE 1
Establishment of a GFP$^-$based system for tracking *Foxp3*-deficient Tregs. **(A)** Schematic illustration of F-KO-BAC and FB-KO-BAC mouse generation. **(B)** Schematic illustration of the GFP$^-$based tracking system of F-KO-BAC and FB-KO-BAC mice. **(C,D)** Representative flow cytometry plot **(C)** or quantification **(D)** of Foxp3$^+$ CD4$^+$ cells. **(E,F)** Representative flow cytometry plot **(E)** or quantification **(F)** of GFP$^+$ CD4$^+$ cells. Each dot in the graphs represents an individual mouse, and the horizontal lines represent means ± SEM. Statistical analysis was performed using the Student's t-test. GFP, green fluorescent protein; Foxp3, forkhead box P3; CD, cluster of differentiation; SEM, standard error of the mean.

were specifically upregulated in FB-KO-BAC cells (FB-KO-UP genes) were found (Figure 2B). Considering that B-cell lymphoma 6 (BCL6) functions as a transcriptional repressor, the study hypothesized that FB-KO-UP genes represent a pathogenic gene expression program in Tregs associated with dermatitis development. To investigate the biological functions enriched in the FB-KO-UP genes, gene ontology (GO) analysis was performed. This revealed an unexpectedly pronounced enrichment of gene signature associated to antiviral and type I IFN signal responses (Figure 2C). This finding was further confirmed via gene set enrichment analysis (GSEA) [28] comparing F-KO-BAC and FB-KO-BAC cells (Figure 2D). In addition, most genes associated with the IFN-alpha response showed the highest expression in the FB-KO-BAC group (Figure 2E). In contrast, reanalysis of GSE40493, a publicly available gene expression dataset comparing Bcl6-deficient and wild-type Tregs [29], showed that GO terms associated with antiviral and type I interferon responses were not significantly enriched in Tregs

10.3389/jcia.2026.17310

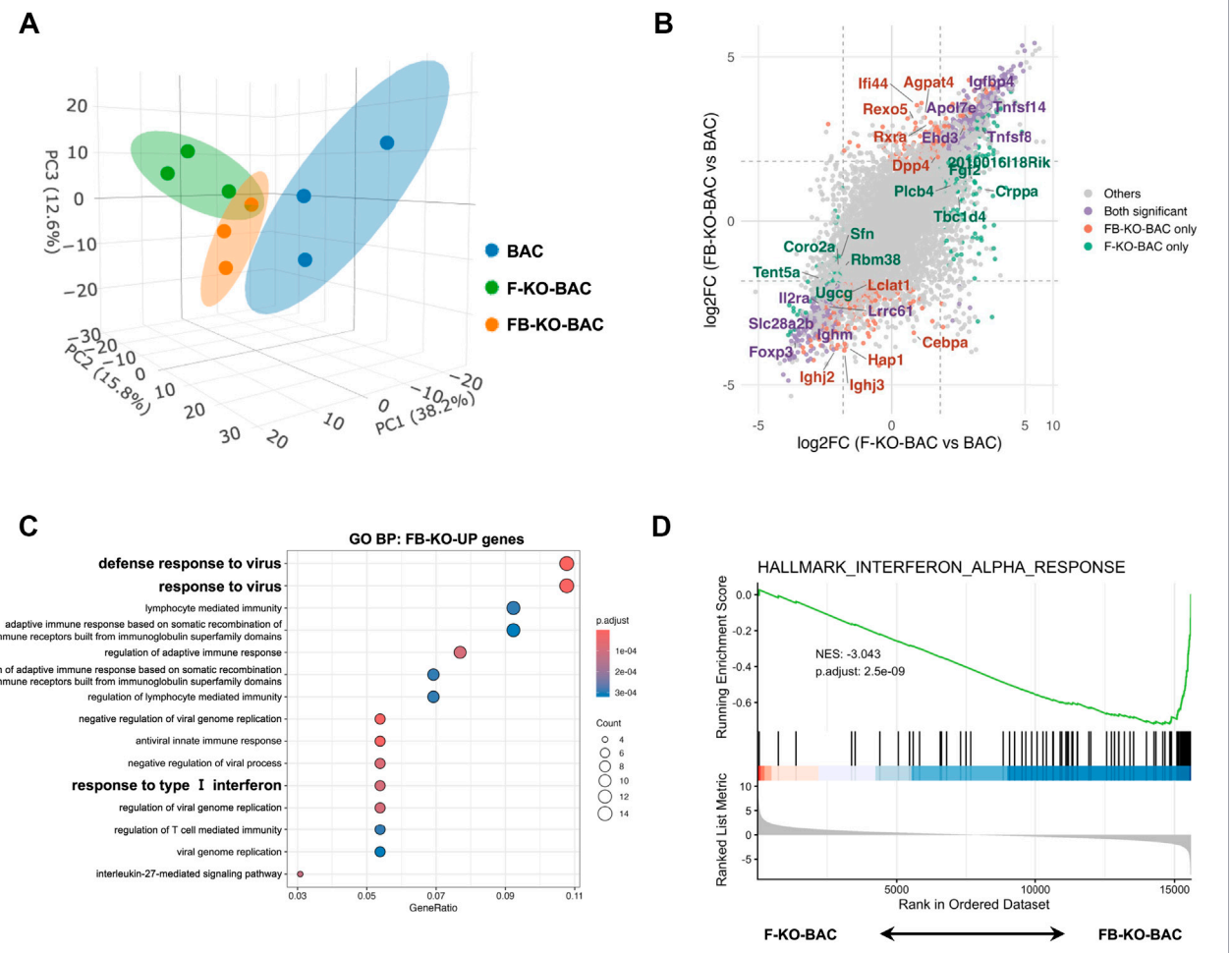

FIGURE 2
Transcriptomic analysis of GFP$^+$ cells. **(A)** PCA of global gene expression in BAC, F-KO-BAC, and FB-KO-BAC cells. **(B)** Scatter plot showing the fold changes of all genes in F-KO-BAC and FB-KO-BAC cells relative to BAC cells. **(C)** Dot plot of GO BP analysis in FB-KO-UP genes. **(D)** GSEA enrichment plot of the Hallmark IFN alpha response gene set comparing FB-KO-BAC cells with F-KO-BAC cells. **(E)** Heatmap showing the expression of genes in the Hallmark IFN alpha response gene set across BAC, F-KO-BAC, and FB-KO-BAC cells. GFP, green fluorescent protein; PCA, principal component analysis; GO, gene ontology; BP, biological process; FB-KO-UP, genes upregulated in FB-KO-BAC cells; GSEA, gene set enrichment analysis.

TABLE 1 GO enrichment analysis of antiviral and type I interferon response pathways in Bcl6-deficient Tregs from GSE40493.

GO term	Gene count	Gene ratio	P. Adjust	Gene name
Response to virus	4	0.0740741	0.095994515	Penk/Fgl2/Gata3/Gbp7
Defense response to virus	2	0.037037	0.283609225	Fgl2/Gbp7
Cellular response to virus	1	0.0185185	0.221601357	Penk
Response to type I interferon	0	0	NA	NA
Cellular response to type I interferon	0	0	NA	NA
Type I interferon-mediated signaling pathway	0	0	NA	NA
Response to interferon-alpha	1	0.0185185	0.173981587	Gata3
Response to interferon-beta	1	0.0185185	0.259668785	Gbp7
Cellular response to interferon-alpha	1	0.0185185	0.147261241	Gata3

GO, Gene Ontology.

lacking Bcl6 alone (Table 1). Collectively, these results indicated that type I IFN-associated gene signature was upregulated in GFP$^+$ Tregs from FB-KO-BAC mice.

Comparison with Treg gene expression profiles in patients with AD

To determine the association between FB-KO-UP genes and the transcriptional state of Tregs in patients with AD, publicly available single-cell RNA-seq (scRNA-seq) data (GSE189188) from patient peripheral blood mononuclear cells (PBMCs) were reanalyzed. All cells that passed quality control were integrated and clustered using Harmony [23]. Major PBMC populations were annotated manually based on canonical marker gene expression and cluster-specific marker genes identified using Seurat's FindAllMarkers function and divided into eight major populations (Figure 3A). "T cells" were then extracted and subjected to reclustering. Based on the identification of cluster-specific marker genes (Figure 3C), the T cell compartment was further subdivided into nine subsets, including "Regulatory T" reflecting Tregs (Figure 3B). Among the 144 FB-KO-UP genes, the study focused on 102 genes that could be successfully converted into human orthologs using GeneToList [24]. Thereafter, the signature score for this gene set was calculated in each T cell cluster, and the differences between the scores of patients with AD and healthy controls (HC) were evaluated. The signature score within the Treg population was substantially higher in the AD group than in the HC group (Figure 3D). Similarly, when the same analysis was applied to the genes included in the GO Biological Process term response to type I IFN, the signature score within Tregs was substantially elevated in the AD group only (Figure 3E). Collectively, these findings indicated that both the FB-KO-UP genes and the type I IFN signature were specifically enriched in Tregs from patient PBMCs.

Identification of a shared upstream transcription factor associated with the gene expression program in FB-KO-BAC and patient Tregs

The recapitulation of upstream transcription factors and their gene regulatory networks (GRN) responsible for the induction of FB-KO-UP genes was assessed in patient Tregs. To identify the major upstream transcription factors driving FB-KO-UP genes, ChIP-X Enrichment Analysis 3 (ChEA3) analysis [30] was performed. Among the top-ranked factors, several were associated with type I IFN signaling, including members of the signal transducer and activator of transcription (STAT) and IRF families. The top 20 major transcription factors are listed in Table 2, and their GRNs in the Treg population were examined using single-cell regulatory network inference and clustering (SCENIC) [25] based on scRNA-seq data. Of the top 20 major transcription factors, nine were detected as regulons by SCENIC, thus enabling the visualization of their GRNs with high regulon activity in AD (Figure 4A). To further evaluate the disease relevance of these regulons, the regulon specificity scores (RSS) [26] were calculated for Tregs from HCs and patients with AD. This analysis showed that most ChEA3-prioritized regulons were preferentially enriched in patient Tregs, with basic leucine zipper ATF-like transcription factor, IRF7, IRF9, STAT2, and STAT1 ranking prominently among the AD-associated regulons. (Figures 4B,C). Collectively, these findings suggest that a subset of the upstream transcriptional regulators implicated in the FB-KO-UP gene program are recapitulated in patient Tregs, where they form disease-associated regulatory networks.

Discussion

This study established a mouse model that enables GFP-based tracking of Tregs, even after inducible deletion of endogenous *Foxp3*. Thereafter, this system was used to characterize the transcriptional consequences of combined *Foxp3* and *Bcl6* deficiency. GFP$^+$ cells from FB-KO-BAC mice acquired a gene expression program enriched for antiviral and type I IFN-related pathways. Importantly, this transcriptional program was not confined to the mouse model but was also selectively enriched in Tregs from patients with AD. Furthermore, upstream regulatory analysis suggested that type I IFN-associated transcription factors, including IRF7, IRF9, STAT1, and STAT2, may have contributed to this shared gene expression program. These findings suggest that the systemic disruption of *Foxp3* and *Bcl6* in Tregs induces a disease-relevant transcriptional state in patients with AD.

10.3389/jcia.2026.17310

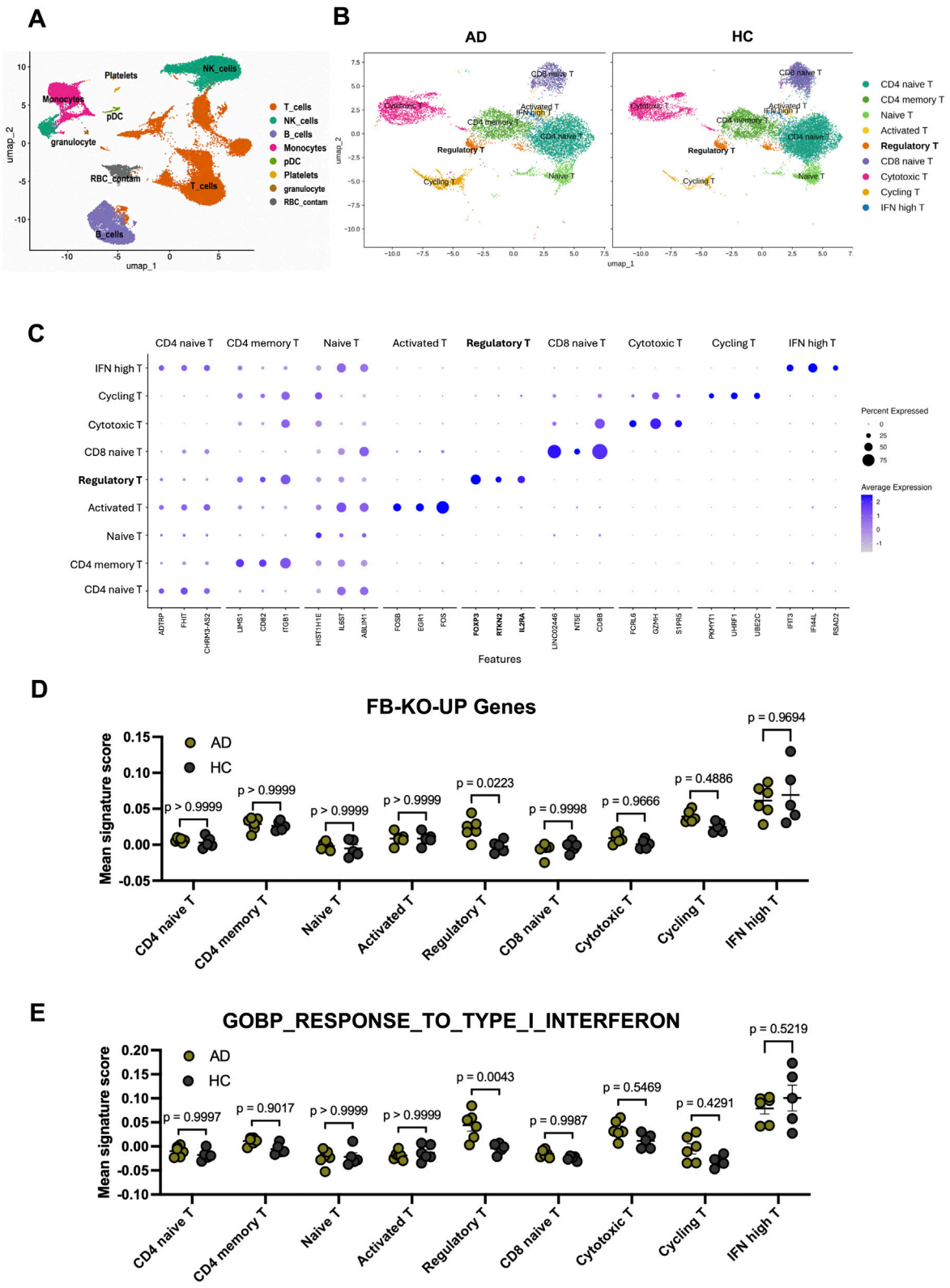

FIGURE 3
Single-cell RNA-seq analysis of GSE189188. **(A)** UMAP visualization of Harmony-integrated PBMC single-cell RNA-seq data. **(B)** UMAP visualization of T cell clusters. **(C)** Dot plot showing representative marker gene expression across T-lineage clusters. Dot size indicates the percentage of cells expressing each gene, and color indicates scaled average expression. **(D,E)** Comparison of FB-KO-UP genes **(D)** or GO BP Response to Type I IFN **(E)** signature scores. Each dot represents one individual, and horizontal lines indicate the mean ± SEM. Statistical analysis was performed using two-way ANOVA followed by *post hoc* t-tests. RNA-seq, RNA sequencing; UMAP, Uniform Manifold Approximation and Projection; FB-KO-UP, genes upregulated in FB-KO-BAC cells; GO, gene ontology, BP, biological process; HC, healthy control; SEM, standard error of the mean; ANOVA, analysis of variance.

TABLE 2 Top 20 major upstream transcriptional factors of FB-KO-UP genes according to ChEA3 analysis.

TF	Mean rank	# of Overlapping Genes	Overlapping Genes
BATF3	16.67	23	IL10,RTP4,PTGIR,GRAMD1A,RSAD2,MX2,ARID5A,IFI44,IFIT1,USP18,IFIT3,PARP12,ARL4C,CCND2,BCL6,OAS2,OAS3,DDIT4,IRF7,CMPK2,CD226,VIM,IL7R
STAT1	17	38	LGALS3BP,RTP4,GRAMD1A,PCNA,DAPL1,TIMM10,IFIT1,USP18,IFIT3,LMNB1,PIK3R5,PREX1,CCND2,ANXA6,METTL9,FNIP2,HERC6,IL10,TIPIN, PTGIR,RSAD2,MX2,ARID5A,OSM,IFI44,CDC7,PARP12,BCL6,OAS2,OAS3,DDIT4,IRF7,CMPK2,CD226,VIM,IL7R,XAF1,GCLM
CENPA	18.5	9	TIPIN,KIF18A,TFDP1,PCNA,CENPW,CDKN2C,OAS2,UBE2T,LMNB1
PLSCR1	20.5	20	RTP4,GRAMD1A,RSAD2,MX2,ARID5A,OSM,IFI44,IFIT1,KMO,USP18,PARP12,IFIT3,PIK3R5,OAS2,CPD,OAS3,IRF7,CMPK2,XAF1,HERC6
IRF9	24	30	RTP4,LGALS3BP,SDC3,TIMM10,OPLAH,IFIT1,USP18,IFIT3,PIK3R5,PDLIM1,PREX1,CCND2,ERI2,HERC6,RSAD2,MX2,TSC22D3,ARID5A,IFI44,NAV1,PARP12, BCL6,OAS2,OAS3,DDIT4,IRF7,CMPK2,VIM,XAF1,IL7R
BATF2	25.67	19	RTP4,LGALS3BP,GRAMD1A,RSAD2,MX2,ARID5A,IFI44,IFIT1,USP18,PARP12,IFIT3,SCML4,OAS2,OAS3,IRF7,CMPK2,IL7R,XAF1,HERC6
SP110	27	22	LGALS3BP,RTP4,RIPOR2,RSAD2,MX2,ARID5A,IFI44,IFIT1,USP18,IFIT3,PARP12,PIK3R5,SCML4,BCL6,OAS2,OAS3,IRF7,CMPK2,VIM,IL7R,XAF1,HERC6
STAT2	27.8	25	LGALS3BP,RTP4,IFIT1,USP18,IFIT3,PDLIM1,CCND2,HERC6,RSAD2,TSC22D3,MX2,ARID5A,IFI44,PARP12,BCL6,OAS2,OAS3, DDIT4,IRF7,CMPK2,VIM,XAF1,IL7R,GCLM,VCL
SP140	28.67	22	LGALS3BP,RTP4,RIPOR2,RSAD2,MX2,ARID5A,IFI44,IFIT1,USP18,IFIT3,PARP12,PIK3R5,LMNB1,PREX1,SCML4,OAS2,OAS3,IRF7,CMPK2,IL7R,XAF1,HERC6
SP100	28.67	21	RTP4,LGALS3BP,RIPOR2,RSAD2,MX2,IFI44,IFIT1,USP18,PARP12,IFIT3,BCL6,OAS2,OAS3,DDIT4,IRF7,CMPK2,CD226,VIM,IL7R,XAF1,HERC6
IRF7	30.33	21	RTP4,LGALS3BP,GRAMD1A,RSAD2,MX2,IFI44,IFIT1,USP18,IFIT3,PARP12,PIK3R5,LMNB1,BCL6,OAS2,OAS3,DDIT4,CMPK2,VIM,IL7R,XAF1,HERC6
ZNF267	31	21	RIPOR2,RSAD2,MX2,TSC22D3,ARID5A,OSM,IFI44,IFIT1,KMO,IFIT3,PIK3R5,LMNB1,ARL4C,CCND2,BCL6,OAS2,DDIT4,IRF7,CMPK2,IL7R,XAF1
BATF	32.2	30	RTP4,RIPOR2,GRAMD1A,IFIT1,IQGAP2,IFIT3,PIK3R5,LMNB1,PLAC8,CCND2,ERI2,ENC1,ANXA6,IL10,TIPIN,RSAD2,MX2,TSC22D3,ARID5A,IFI44, PARP12,BCL6,OAS2,OAS3,DDIT4,IRF7,CD226,VIM,IL7R,XAF1
ETV3L	33	21	IL10,HS3ST3B1,PTGIR,GRAMD1A,PCNA,RSAD2,OSM,IFI44,NAV1,IFIT1,KMO,USP18,IFIT3,OAS2,OAS3,DDIT4,IRF7,CMPK2,CD226,IL7R,IL9R
RELB	36	29	LGALS3BP,RTP4,GRAMD1A,PCNA,IFIT1,CRIP1,USP18,IFIT3,PIK3R5,ENC1,ANXA6,PDLIM4,NPDC1,TIPIN,RSAD2,MX2,TSC22D3,ARID5A,IFI44, PARP12,ARL4C,BCL6,OAS2,OAS3,DDIT4,IRF7,VIM,IL7R,XAF1
IRF4	44.6	30	RIPOR2,PRIM2,PCNA,IQGAP2,USP18,IFIT3,LMNB1,PIK3R5,DPP4,CCND2,ENC1,ANXA6,HERC6,IL10,RSAD2,MX2,F2R,ARID5A,ARL4C,TFDP1,BCL6,OAS2,OAS3, DDIT4,IRF7,CMPK2,CD226,VIM,IL7R,IL9R
IRF1	45.17	44	LGALS3BP,RTP4,PRIM2,RIPOR2,GRAMD1A,PCNA,IFIT1,OPLAH,CRIP1,USP18,IFIT3,PIK3R5,AGPAT4,UNG,PREX1,CCND2,SCML4,P2RY1,HERC6, TIPIN,CDKN2C,CENPW,RSAD2,MX2,TSC22D3,F2R,OSM,IFI44,REXO2,PARP12,KIF18A,BCL6,OAS2,OAS3,CPD,CYP2S1,MGAT4A,DDIT4,IRF7,CMPK2, CD226,VIM,IL7R,XAF1
IKZF2	45.33	24	RIPOR2,PCNA,RSAD2,IFI44,NAV1,IFIT1,IQGAP2,USP18,IFIT3,LMNB1,DPP4,ARL4C,CCND2,BCL6,OAS2,OAS3,MGAT4A,DDIT4,ANXA6, CD226,VIM,IL7R,XAF1,IL9R
ZNF367	47.33	15	TIPIN,DUT,PCNA,CENPW,CDKN2C,CTDSPL,CDC7,LMNB1,UNG,KIF18A,TFDP1,UBE2T,DDIT4,CD226,VCL
E2F1	47.33	29	PCNA,SDC3,CRIP2,CRIP1,USP18,LMNB1,CIART,UNG,PREX1,CCND2,HECTD2,ERI2,METTL9,TIPIN,DUT,CENPW,CDKN2C,PAQR4,CDC7,MANEAL,ABHD15, ACAP3,SQLE,KIF18A,TFDP1,UBE2T,OAS3,DDIT4,MNS1

ChEA3, ChIP-X Enrichment Analysis 3.

10.3389/jcia.2026.17310

Foxp3-deficient mice [31] and scurfy mice [32] develop systemic autoimmunity and undergo early disease development. This renders examining immune state transitions in a temporally controlled manner during disease development difficult. Therefore, a tamoxifen-inducible conditional knockout strategy was used. However, the conditional loss of *Foxp3* indicates that these cells can no longer be readily identified as Tregs using conventional approaches. The use of inducible Foxp3 protein-degradation systems overcomes this limitation and provides important insights into the phenotypic changes that occur after *Foxp3* loss [33, 34]. In particular, the rapid loss of C-X-C motif chemokine receptor 3-positive Tregs following Foxp3 protein degradation, a subset capable of migrating to inflammatory sites, suggests that the loss of *Foxp3* substantially alters the *in vivo* distribution of Tregs [34]. Hence, the current study model offers several complementary advantages. Given that the BAC transgene enables *Foxp3* promoter-dependent expression of luciferase and GFP, it permits isolation of *Foxp3*-deficient Tregs and longitudinal tracking of the redistribution of these cells *in vivo* after *Foxp3* loss. Such an approach may be particularly valuable for defining the effects of *Foxp3* loss on the tissue distribution, persistence, and disease-associated state transitions of Tregs during dermatitis development.

Although Tregs are essential for the maintenance of immune tolerance in barrier tissues, their role in AD remains unclear. $FOXP3^+$ Tregs increase in severe AD [10], which suggests that Tregs in AD are functionally altered rather than simply insufficient in number. In accordance, gene expression changes have been observed in transcriptomic analyses of Tregs derived from PBMCs of patients with AD, thus suggesting impaired immunosuppressive function [11]. These findings suggest that dysfunctional Tregs contribute to AD pathogenesis. Therefore, tracing the phenotypic and transcriptional changes in Tregs during disease development and identifying the key stages contributing to disease pathogenesis will provide important insights into Treg-targeted therapeutic strategies. The most widely used MC903-induced AD model exhibits extremely rapid disease progression [13]. This renders evaluation of the relationship between endogenous immune states and disease development difficult. In contrast, the current study model requires approximately 2 weeks from gene deletion until the onset of dermatitis [16]. This enables detailed tracking of phenotypic changes in Tregs before and after disease onset. Furthermore, disease stage-specific depletion of Tregs allows direct assessment of their functional contribution to disease initiation and progression. Analyses using this model will enhance current understanding of the mechanisms by which Tregs regulate AD pathogenesis and provide valuable insights into novel therapeutic strategies.

In the transcriptomic analysis, the additional deletion of *Bcl6* enhanced type I IFN-associated gene signature compared with that under *Foxp3* deletion alone. BCL6 is a transcriptional repressor that suppresses antiviral and type I IFN-associated gene programs in several cell types, including macrophages [35] and T follicular helper cells [36]. Therefore, this signature could potentially reflect the effect of *Bcl6* deficiency. However, reanalysis of publicly available transcriptional data [29] revealed that Bcl6-deficient Tregs did not show clear enrichment of type I IFN signaling. These observations suggest that loss of Bcl6 alone is insufficient to reproduce the transcriptional program observed in FB-KO-BAC Tregs. Rather, disruption of both $Foxp3^-$ and Bcl6-dependent transcriptional control may create a Treg state permissive for the emergence of an IFN-associated gene expression program in this lineage.

Although AD is predominantly characterized by type 2 inflammation [2], type I IFNs have a complex role in its pathophysiology. Impaired antiviral immunity is a well-recognized feature of AD, particularly in patients susceptible to eczema herpeticum [37]. In addition, plasmacytoid dendritic cells, a major source of type I IFNs, are markedly reduced in AD skin, which may contribute to impaired cutaneous antiviral defense [38]. Consistent with a protective role of type I IFNs in AD, experimental studies have shown that these cytokines can suppress type 2 inflammation in AD-like dermatitis. For example, Miyagawa et al. demonstrated that type I IFN produced by $Ly6C^{hi}$ monocytes limited type 2 inflammation in a murine AD model, whereas disruption of this pathway exacerbated disease [39]. Together, these studies suggest that insufficient type I IFN activity may contribute to impaired antiviral defense and enhanced type 2 inflammation in AD. In contrast, our analysis identified an IFN-associated transcriptional signature specifically in Tregs from patients with AD. This apparent discrepancy suggests that type I IFN-related responses in AD may differ among cell types, with Tregs acquiring an IFN-responsive transcriptional state even when overall antiviral immunity is impaired.

The upstream regulatory analysis further places this Treg state within a canonical type I IFN-associated transcriptional network. Type I IFNs activate JAK–STAT signaling, leading to the formation of the ISGF3 complex composed of STAT1, STAT2, and IRF9, which induces a broad repertoire of IFN-stimulated genes [40]. IRF7 functions as an important amplifier of this antiviral transcriptional program [41]. Consistent with this framework, the present analysis identified enrichment of IRF7-, IRF9-, STAT1-, and STAT2-associated regulons in AD Tregs, together with increased expression of IFN-related genes. The coordinated enrichment of these regulators is therefore consistent with acquisition of type I IFN-responsive transcriptional state, although the transcriptomic data alone do not establish functional activation of its downstream signaling.

Previous studies indicate that the consequences of type I IFN signaling in Tregs are strongly context-dependent. During rhinovirus infection, human Tregs acquire an antiviral transcriptional program characterized by increased IRF7, ISG15, MX1, IFI44L, and STAT1 expression, accompanied by reduced suppressive capacity [42]. Similarly, a recent single-cell analysis of chronic immune thrombocytopenia identified expansion of an IFN signature-high Treg population, in which the IFN-stimulated gene RSAD2/Viperin contributed to impaired Treg function [43]. These observations are consistent with the IFN-associated transcriptional state observed in AD Tregs in the present study. However, the effects of type I IFN signaling on Tregs are not uniformly detrimental. Treg-specific IFNAR signaling has also been shown to promote Treg development and peripheral survival under certain conditions [44]. Thus, the biological consequence of an IFN-associated transcriptional state appears to depend strongly on the inflammatory setting. This interpretation is also relevant to previous observations of Treg abnormalities in AD. $FOXP3^+$ Tregs are expanded in severe AD [10], indicating that disease-associated Treg abnormalities cannot be explained simply by a numerical deficiency. Reduced suppressive capacity and altered CTLA-4-dependent regulation have also been reported in Tregs from patients with AD [11]. Type I IFN-associated transcriptional

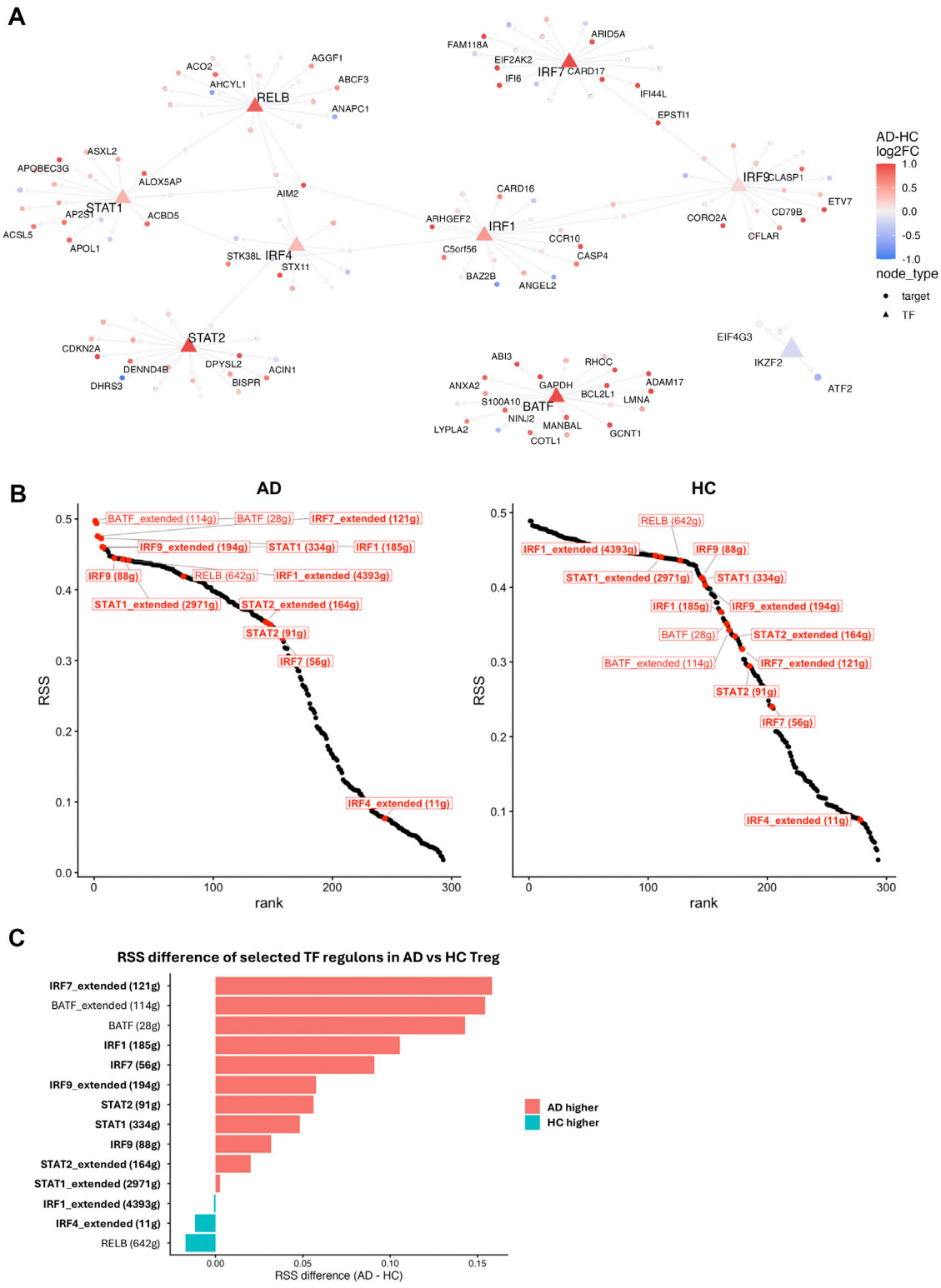

FIGURE 4
Analysis of GRNs via SCENIC. **(A)** GRN visualization of ChEA3-prioritized transcription factors detected as SCENIC regulons in Tregs. **(B)** RSS ranking plots showing regulon enrichment in Tregs from patients with AD and HC. ChEA3-prioritized transcription factors are highlighted. **(C)** Bar plot showing differences in RSS between AD and HC Tregs for ChEA3-prioritized transcription factors. GRN, gene regulatory network; SCENIC, single-cell regulatory network inference and clustering; ChEA3, ChIP-X Enrichment Analysis 3; RSS, regulon specificity scores; HC, healthy control.

state identified here may therefore represent one molecular feature of the altered Treg states previously described in AD. However, because suppressive activity was not directly assessed in the human Tregs analyzed in the present study, it remains unknown whether the type I IFN-associated program is mechanistically responsible for Treg dysfunction in AD.

The present study extends these previous observations in two important respects. First, whereas type I IFN-responsive Treg states have mainly been characterized in viral infection and systemic immune disorders, the current analysis identifies a related transcriptional state in Tregs from patients with AD, a predominantly type 2 and noninfectious inflammatory skin disease. Second, cross-species analysis links this human Treg state to a genetically defined spontaneous dermatitis model in which combined Foxp3 and Bcl6 deficiency produces a similar type I IFN-associated gene expression program and upstream regulon profile. These findings suggest that type I IFN-associated transcriptional signature can emerge in Tregs under chronic type 2 inflammation and disrupted Treg regulation, and may represent a disease-associated state conserved across species.

Nevertheless, several limitations of the present study should be acknowledged. First, although the majority of $CD4^+GFP^+$ cells in untreated FB-KO-BAC mice exhibited a conventional Treg phenotype, approximant 10% was $Foxp3^-$. Therefore, a minor contribution of non-Treg cells to the GFP^+ population and the resulting transcriptomic profiles cannot be completely excluded. The development or use of a more Treg-specific reporter system would enable more precise tracking and molecular characterization of Tregs after Foxp3 deletion. Second, although $CD4^+GFP^+$ cells were detected in lesional skin of FB-KO-BAC mice, their direct contribution to dermatitis remains unclear. Whether these cells promote disease through the production of specific cytokines or other effector molecules was not determined. Functional analyses of lesional GFP^+ cells, together with cell-specific depletion or manipulation, will be required to establish their causal role in disease development. Third, the human transcriptomic analysis in the present study was restricted to AD. Therefore, it remains unclear whether the type I IFN-associated Treg state identified here is specific to AD or represents a more general feature of inflammatory skin diseases. Comparative analyses of Tregs across other skin disorders will be necessary to determine the disease specificity of this transcriptional state.

Data availability statement

The datasets presented in this study can be found in online repositories. The names of the repository/repositories and accession number(s) can be found below: https://www.ncbi.nlm.nih.gov/, PRJNA1473592.

Ethics statement

All animal experiments were approved by the Animal Experimentation Committee of Tokyo University of Science (approval number: Y25018). All experiments were conducted in accordance with the Animal Research: Reporting of In Vivo Experiments (ARRIVE) guidelines established by the National Center for the Replacement, Refinement, and Reduction of Animals in Research (NC3Rs).

Author contributions

NK: Conceptualization, Methodology, Data curation, Writing – original draft, Formal analysis, and Investigation. HN, CN, MS, MB, and RK: Data curation, Formal analysis, and Investigation. YH: Conceptualization, Methodology, Resources, Writing – original draft, and Writing – review and editing. All authors contributed to the article and approved the submitted version.

Funding

The author(s) declared that financial support was received for this work and/or its publication. This work was supported by the Japan Society for the Promotion of Science (JSPS) KAKENHI (Grant Number 23K06599 to YH).

Acknowledgments

We thank Riyo Kawasaki for providing technical support. We also thank Dr. Toshitada Takemori for providing $Bcl6^{flox}$ mice, Dr. Thomas Ludwig for providing $R26^{CreERT2}$ mice, and Dr. Günter J. Hämmerling for providing Foxp3.LuciDTR mice.

Conflict of interest

The author(s) declared that this work was conducted in the absence of any commercial or financial relationships that could be construed as a potential conflict of interest.

Generative AI statement

The author(s) declared that generative AI was used in the creation of this manuscript. During the preparation for this study, the authors used ChatGPT (OpenAI) for English language editing and grammar checking. After using this tool, the authors reviewed and edited the content as needed and take full responsibility for the content of the publication.

Any alternative text (alt text) provided alongside figures in this article has been generated by Frontiers with the support of artificial intelligence and reasonable efforts have been made to ensure accuracy, including review by the authors wherever possible. If you identify any issues, please contact us.

Supplementary material

The Supplementary Material for this article can be found online at: https://www.frontierspartnerships.org/articles/10.3389/jcia.2026.17310/full#supplementary-material

References

1. Yang G, Seok JK, Kang HC, Cho YY, Lee HS, Lee JY. Skin barrier abnormalities and immune dysfunction in atopic dermatitis. *Int J Mol Sci* (2020) 21(8):2867. doi: 10.3390/ijms21082867

2. Ogulur I, Mitamura Y, Yazici D, Pat Y, Ardicli S, Li M, et al. Type 2 immunity in allergic diseases. *Cell Mol Immunol* (2025) 22(3):211–42. doi: 10.1038/s41423-025-01261-2

3. Beck LA, Bissonnette R, Deleuran M, Nakahara T, Galus R, Coleman A, et al. Dupilumab in adults with moderate to severe atopic dermatitis: a 5-Year open-label extension study. *JAMA Dermatol* (2024) 160(8):805–12. doi: 10.1001/jamadermatol.2024.1536

4. Simpson EL, Bieber T, Guttman-Yassky E, Beck LA, Blauvelt A, Cork MJ, et al. Two phase 3 trials of dupilumab *versus* placebo in atopic dermatitis. *N Engl J Med* (2016) 375(24):2335–48. doi: 10.1056/NEJMoa1610020

5. Boscia G, Spataro F, Desantis V, Solimando AG, Vacca A, Ria R, et al. Ocular side effects of dupilumab: a comprehensive overview of the literature. *J Clin Med* (2025) 14(7):2487. doi: 10.3390/jcm14072487

6. Eyerich K, Gooderham MJ, Silvestre JF, Shumack SP, Mendes-Bastos P, Aoki V, et al. Real-world clinical, psychosocial and economic burden of atopic dermatitis: results from a multicountry study. *J Eur Acad Dermatol Venereol* (2024) 38(2):340–53. doi: 10.1111/jdv.19500

7. Sakaguchi S, Yamaguchi T, Nomura T, Ono M. Regulatory T cells and immune tolerance. *Cell* (2008) 133(5):775–87. doi: 10.1016/j.cell.2008.05.009

8. Conrad ML, Barrientos G, Cai X, Mukherjee S, Das M, Stephen-Victor E, et al. Regulatory T cells and their role in allergic disease. *Allergy* (2025) 80(1):77–93. doi: 10.1111/all.16326

9. Hanafusa T, Matsui S, Murota H, Tani M, Igawa K, Katayama I. Increased frequency of skin-infiltrating FoxP3+ regulatory T cells as a diagnostic indicator of severe atopic dermatitis from cutaneous T cell lymphoma. *Clin Exp Immunol* (2013) 172(3):507–12. doi: 10.1111/cei.12073

10. Roesner LM, Floess S, Witte T, Olek S, Huehn J, Werfel T. Foxp3+ regulatory T cells are expanded in severe atopic dermatitis patients. *Allergy* (2015) 70(12):1656–60. doi: 10.1111/all.12712

11. Kang SJ, Gong JR, Jin SP, Oh JM, Jin H, Lee Y, et al. Deciphering dysfunctional regulatory T cells in atopic dermatitis. *Allergy* (2025) 80(5):1473–7. doi: 10.1111/all.16439

12. Alam MJ, Xie L, Yap YA, Robert R. A mouse model of MC903-Induced atopic dermatitis. *Curr Protoc* (2023) 3(3):e695. doi: 10.1002/cpz1.695

13. Zheng R, Ren Y, Liu X, He C, Liu H, Wang Y, et al. Exogenous drug-induced mouse models of atopic dermatitis. *Cytokine Growth Factor Rev* (2024) 77:104–16. doi: 10.1016/j.cytogfr.2024.01.003

14. Song MH, Gupta A, Sasidharan Nair V, Oh K. CD4+ T cells play an essential role in chronic MC903-induced skin inflammation. *Biochem Biophys Res Commun* (2022) 612:8–14. doi: 10.1016/j.bbrc.2022.04.106

15. Sakamoto K, Nagao K. Mouse models for atopic dermatitis. *Curr Protoc* (2023) 3(3):e709. doi: 10.1002/cpz1.709

16. Tai Y, Sakaida Y, Kawasaki R, Kanemaru K, Akimoto K, Brombacher F, et al. Foxp3 and Bcl6 deficiency synergistically induces spontaneous development of atopic dermatitis-like skin disease. *Int Immunol* (2023) 35(9):423–35. doi: 10.1093/intimm/dxad018

17. Tai Y, Takano A, Haga K, Koshida K, Harada Y. Spontaneous antibody production caused by regulatory T cell deficiency occurs through a germinal center-independent pathway. *Biochem Biophys Res Commun* (2020) 527(4):909–14. doi: 10.1016/j.bbrc.2020.05.026

18. Li Y, Wang Z, Lin H, Wang L, Chen X, Liu Q, et al. Bcl6 preserves the suppressive function of regulatory T cells during tumorigenesis. *Front Immunol* (2020) 11:11. doi: 10.3389/fimmu.2020.00806

19. Suffner J, Hochweller K, Kühnle MC, Li X, Kroczek RA, Garbi N, et al. Dendritic cells support homeostatic expansion of Foxp3+ regulatory T cells in Foxp3.LuciDTR mice. *J Immunol* (2010) 184(4):1810–20. doi: 10.4049/jimmunol.0902420

20. Sakamoto K, Goel S, Funakoshi A, Honda T, Nagao K. Flow cytometry analysis of the subpopulations of mouse keratinocytes and skin immune cells. *STAR Protoc* (2022) 3(1):101052. doi: 10.1016/j.xpro.2021.101052

21. Satija R, Farrell JA, Gennert D, Schier AF, Regev A. Spatial reconstruction of single-cell gene expression data. *Nat Biotechnol* (2015) 33(5):495–502. doi: 10.1038/nbt.3192

22. Stuart T, Butler A, Hoffman P, Hafemeister C, Papalexi E, Mauck WM, et al. Comprehensive integration of single-cell data. *Cell* (2019) 177(7):1888–902.e21. doi: 10.1016/j.cell.2019.05.031

23. Korsunsky I, Millard N, Fan J, Slowikowski K, Zhang F, Wei K, et al. Fast, sensitive and accurate integration of single-cell data with harmony. *Nat Methods* (2019) 16(12):1289–96. doi: 10.1038/s41592-019-0619-0

24. Breidenbach JD, Iii EFB, Kennedy DJ, Haller ST. GeneToList: a web application to assist with gene identifiers for the non-bioinformatics-savvy scientist. *Biology* (2022) 11(8):1113. doi: 10.3390/biology11081113

25. Aibar S, González-Blas CB, Moerman T, Huynh-Thu VA, Imrichova H, Hulselmans G, et al. SCENIC: single-cell regulatory network inference and clustering. *Nat Methods* (2017) 14(11):1083–6. doi: 10.1038/nmeth.4463

26. Suo S, Zhu Q, Saadatpour A, Fei L, Guo G, Yuan GC. Revealing the critical regulators of cell identity in the mouse cell atlas. *Cell Rep* (2018) 25(6):1436–45.e3. doi: 10.1016/j.celrep.2018.10.045

27. Tai Y, Sakamoto K, Takano A, Haga K, Harada Y. Dysregulation of humoral immunity in Foxp3 conditional-knockout mice. *Biochem Biophys Res Commun* (2019) 513(4):787–93. doi: 10.1016/j.bbrc.2019.04.090

28. Liberzon A, Birger C, Thorvaldsdóttir H, Ghandi M, Mesirov JP, Tamayo P. The molecular signatures database hallmark gene set collection. *Cell Syst* (2015) 1(6):417–25. doi: 10.1016/j.cels.2015.12.004

29. Sawant DV, Sehra S, Nguyen ET, Jadhav R, Englert K, Shinnakasu R, et al. Bcl6 controls the Th2 inflammatory activity of regulatory T cells by repressing Gata3 function. *J Immunol Baltim Md* (2012) 189(10):4759–69. doi: 10.4049/jimmunol.1201794

30. Keenan AB, Torre D, Lachmann A, Leong AK, Wojciechowicz ML, Utti V, et al. ChEA3: transcription factor enrichment analysis by orthogonal omics integration. *Nucleic Acids Res* (2019) 47(W1):W212–24. doi: 10.1093/nar/gkz446

31. Fontenot JD, Rasmussen JP, Williams LM, Dooley JL, Farr AG, Rudensky AY. Regulatory T cell lineage specification by the forkhead transcription factor Foxp3. *Immunity* (2005) 22(3):329–41. doi: 10.1016/j.immuni.2005.01.016

32. Brunkow ME, Jeffery EW, Hjerrild KA, Paeper B, Clark LB, Yasayko SA, et al. Disruption of a new forkhead/winged-helix protein, scurfin, results in the fatal lymphoproliferative disorder of the scurfy mouse. *Nat Genet* (2001) 27(1):68–73. doi: 10.1038/83784

33. Hu W, Dolsten GA, Wang EY, Beroshvili G, Wang ZM, Ghelani AP, et al. Temporal and context-dependent requirements for the transcription factor Foxp3 expression in regulatory T cells. *Nat Immunol* (2025) 26(11):2059–73. doi: 10.1038/s41590-025-02295-4

34. Jäger C, Dimitrova P, Sun Q, Tennebroek J, Marchiori E, Jaritz M, et al. Inducible protein degradation reveals inflammation-dependent function of the treg cell lineage–defining transcription factor Foxp3. *Sci Immunol* (2025) 10(108):eadr7057. doi: 10.1126/sciimmunol.adr7057

35. Xu F, Kang Y, Zhuang N, Lu Z, Zhang H, Xu D, et al. Bcl6 sets a threshold for antiviral signaling by restraining IRF7 transcriptional program. *Sci Rep* (2016) 6(1):18778. doi: 10.1038/srep18778

36. Amet T, Son YM, Jiang L, Cheon IS, Huang S, Gupta SK, et al. BCL6 represses antiviral resistance in follicular T helper cells. *J Leukoc Biol* (2017) 102(2):527–36. doi: 10.1189/jlb.4A1216-513RR

37. Bin L, Edwards MG, Heiser R, Streib J, Richers B, Leung DYM. Identification of novel gene signatures in atopic dermatitis complicated by eczema herpeticum. *J Allergy Clin Immunol* (2014) 133(2):AB193. doi: 10.1016/j.jaci.2013.12.690

38. Wollenberg A, Günther S, Moderer M, Wetzel S, Wagner M, Towarowski A, et al. Plasmacytoid dendritic cells: a new cutaneous dendritic cell subset with distinct role in inflammatory skin diseases. *J Invest Dermatol* (2002) 119(5):1096–102. doi: 10.1046/j.1523-1747.2002.19515.x

39. Miyagawa F, Ozato K, Tagaya Y, Asada H. Type I IFN derived from Ly6Chi monocytes suppresses type 2 inflammation in a murine model of atopic dermatitis. *J Invest Dermatol* (2024) 144(3):520–30.e2. doi: 10.1016/j.jid.2023.08.022

40. Wang W, Xu L, Su J, Peppelenbosch MP, Pan Q. Transcriptional regulation of antiviral interferon-stimulated genes. *Trends Microbiol* (2017) 25(7):573–84. doi: 10.1016/j.tim.2017.01.001

41. Ma W, Huang G, Wang Z, Wang L, Gao Q. IRF7: role and regulation in immunity and autoimmunity. *Front Immunol* (2023) 14:1236923. doi: 10.3389/fimmu.2023.1236923

42. Jansen K, Wirz OF, van de Veen W, Tan G, Mirer D, Sokolowska M, et al. Loss of regulatory capacity in treg cells following rhinovirus infection. *J Allergy Clin Immunol* (2021) 148(4):1016–29.e16. doi: 10.1016/j.jaci.2021.05.045

43. Li T, Li X, Huang H, Liu P, Shen Z, Xue C. Interferon-stimulated viperin impairs treg function in autoimmune thrombocytopenia. *Cell Commun Signal* (2025) 23(1):500. doi: 10.1186/s12964-025-02511-6

44. Metidji A, Rieder SA, Glass DD, Cremer I, Punkosdy GA, Shevach EM. IFNα/βR signaling promotes regulatory T cell development and function under stress conditions. *J Immunol Baltim Md* (2015) 194(9):4265–76. doi: 10.4049/jimmunol.1500036